# ENABLING THE PRACTICAL APPLICATION OF OXIDE DISPERSION-STRENGTHENED FERRITIC STEELS

I.G. Wright
Oak Ridge National Laboratory, 1 Bethel Valley Road, MS 6156, Oak Ridge, TN 37831
E-mail: wrightig@ornl.gov; telephone: 865-574-4451; Fax: 865-241-0215

B.A. Pint
Oak Ridge National Laboratory, 1 Bethel Valley Road, MS 6156, Oak Ridge, TN 37831
E-mail: pintba@ornl.gov; telephone: 865-576-2897; Fax: 865-241-0215

E.G. Dyadko
MER Corporation, 7960 S. Kolb Rd., Tucson, AZ 85706
E-mail: edyadko@mercorp.com; telephone: 520-574-1980 x142; Fax: 520-574-1983

N.S. Bornstein
Consultant, 43 Richmond Lane, W. Hartford, CT 06117
E-mail: normanbornstein@sbcglobal.net; telephone: 860-408-1432

G.J. Tatlock
University of Liverpool, Brownlow Hill, Liverpool L69 3GH, England
E-mail: g.j.tatlock@liverpool.ac.uk; telephone: 011-44-151-794-5367; Fax: 011-44-151-794-4675

## ABSTRACT

Effort has continued to evaluate joints made in oxide dispersion-strengthened (ODS) FeCrAl by (i) pulsed plasma-assisted diffusion (PPAD) bonding, and (ii) transient liquid phase (TLP) bonding. Creep tests of PPAD-bonded butt joints in air at 1000°C, using small, shoulder-loaded, dog bone-shaped specimens and an incrementally-loaded test technique, indicated that failure occurred at loads of up to 82% of that required to fail the parent alloy in the same test. For high creep-strength ferritic steels joined by conventional welding methods, failure at loads of 50-80% that required to fail the parent alloy ('strength reduction factors') are considered to be acceptable. The failures apparently did not initiate along the joints; the observed mode of failure of the joined specimens was the same as observed for monolithic specimens of this alloy, by crack-initiated transgranular brittle fracture, followed by ductile overload failure. The progress of TLP bonding has been slower, with the major effort focused on understanding the behavior of the transient liquid phase and its interaction with the alloy microstructure during the various stages of bonding. Creep testing using the same procedures also has been used to evaluate changes resulting from torsional deformation of ODS-FeCrAl tubes in an attempt to modify their microstructures and increase their hoop strength. Interpretation of the results so far has not shown a clear trend, largely due to difficulties in measuring the effective angle of twist in the specimen gauge lengths. Other issues that have been addressed are the refinement of an approach for prediction of the oxidation-limited service lifetime of alumina scale-forming ODS alloys, and alternative routes for ODS alloy powder processing. Analysis of alloy specimens oxidized to failure (in some cases involving exposures for many thousands of hours) over a range of temperatures has provided an improved basis for calculating the values of parameters required in the lifing model (minimum Al content for protective behavior; initiation point for scale spallation); a quantitative description of the influence of specimen shape remains to be addressed.

## INTRODUCTION

ODS alloys have distinct advantages over conventional high-temperature alloys in that they exhibit creep strength at significantly higher temperatures, and have exceptional inherent resistance to high-temperature oxidation in terms of rate of scale growth and scale adherence due to the formation of $\alpha$-$Al_2O_3$ scales [1]. Because of these properties, ODS alloys provide an alternative choice for the lower end of the temperature range usually attributed to ceramics. There is currently a resurgence of industrial interest in ODS alloys for applications ranging from high-temperature heat exchangers for indirect preheating of steam or $H_2$ for gasification of coal, and for heat recuperation in fossil fuel-fired metal smelters and melters, to use as a replacement for refractories used for containment of molten metal in the production of $H_2$ from coal [2]. There is also renewed interest in the use of ODS alloys for airfoils for use at the higher temperatures anticipated in gas turbines burning syngas with variable quantities of $H_2$ [3].

The barriers that have prevented the broad application of ODS alloys still are centered around cost (since ODS alloy production involves a powder metallurgical route), and the fact that they cannot be joined by conventional fusion welding (since the fine dispersion of oxides typically agglomerates in the fusion zone, leaving a joint which may be an order of magnitude lower in high-temperature creep strength than the monolithic alloy [4-6]). Other joining methods involving brazing or diffusion bonding have been demonstrated with some success [5,7-10], particularly with B-containing brazing alloys. A common difficulty was obtaining grain growth across the bond, and no creep data have been reported to indicate that extent of strength reduction. Three methods which do not involve the addition of an extra filler material recently have shown promise: friction stir welding [11,12]; solid-state diffusion bonding (joints in alloy PM2000 exhibited 70% of the room-temperature shear strength of the parent alloy [13]); and pulsed plasma-assisted diffusion bonding [14]. Progress in transient liquid-phase (TLP) bonding and pulsed plasma-assisted diffusion (PPAD) bonding are reported.

Since ODS-FeCrAl alloys form very thin, protective alumina scales that are uniform in thickness with negligible internal attack, it is difficult to estimate service lifetime from readily-measurable parameters such as section thinning. Because of the very well-controlled oxidation behavior, and since the Al concentration gradient in the alloy is essentially flat (in many cases) until very near the end of life, a relatively straightforward basis for predicting the oxidation-limited lifetimes of these alloys is possible by equating the oxidation lifetime to the rate of consumption of the available Al to form the alumina scale [15,16]. Progress in measuring some of these parameters is reported.

## RESULTS AND DISCUSSION

### JOINING

Transient Liquid-Phase (TLP) Bonding

Further characterization of the TLP bonds described earlier [17] was made to determine the effects of heat treatment on homogenizing the composition in the vicinity of the bonds, and on the microstructure of the alloy. A specimen cut from a block of unrecrystallized alloy PM2000 (condition KKL4) that had been bonded using the original TLP foil, was subjected to the standard recrystallization anneal for alloy PM2000 (1h at 1380°C). The appearance of the bond, shown in Fig. 1a, indicates some porosity (or incomplete bonding) near the edges of the specimen whereas, near the center of the specimen, the bond line was demarcated by a change in alloy grain structure (Figs. 1 b and c), and any associated porosity was very fine. The backscattered electron (BSE) image of a similar section of the bond from examination in a scanning electron microscope (SEM), shown in Fig. 1d, indicates that some alloy grain growth had occurred in the immediate vicinity of the bond line, extending approximately 100 $\mu$m into the alloy, but that secondary recrystallization of the bulk of the alloy had not proceeded to produce the desired large grain structure. A particularly notable feature was that the bright-appearing (element X-rich) precipitates

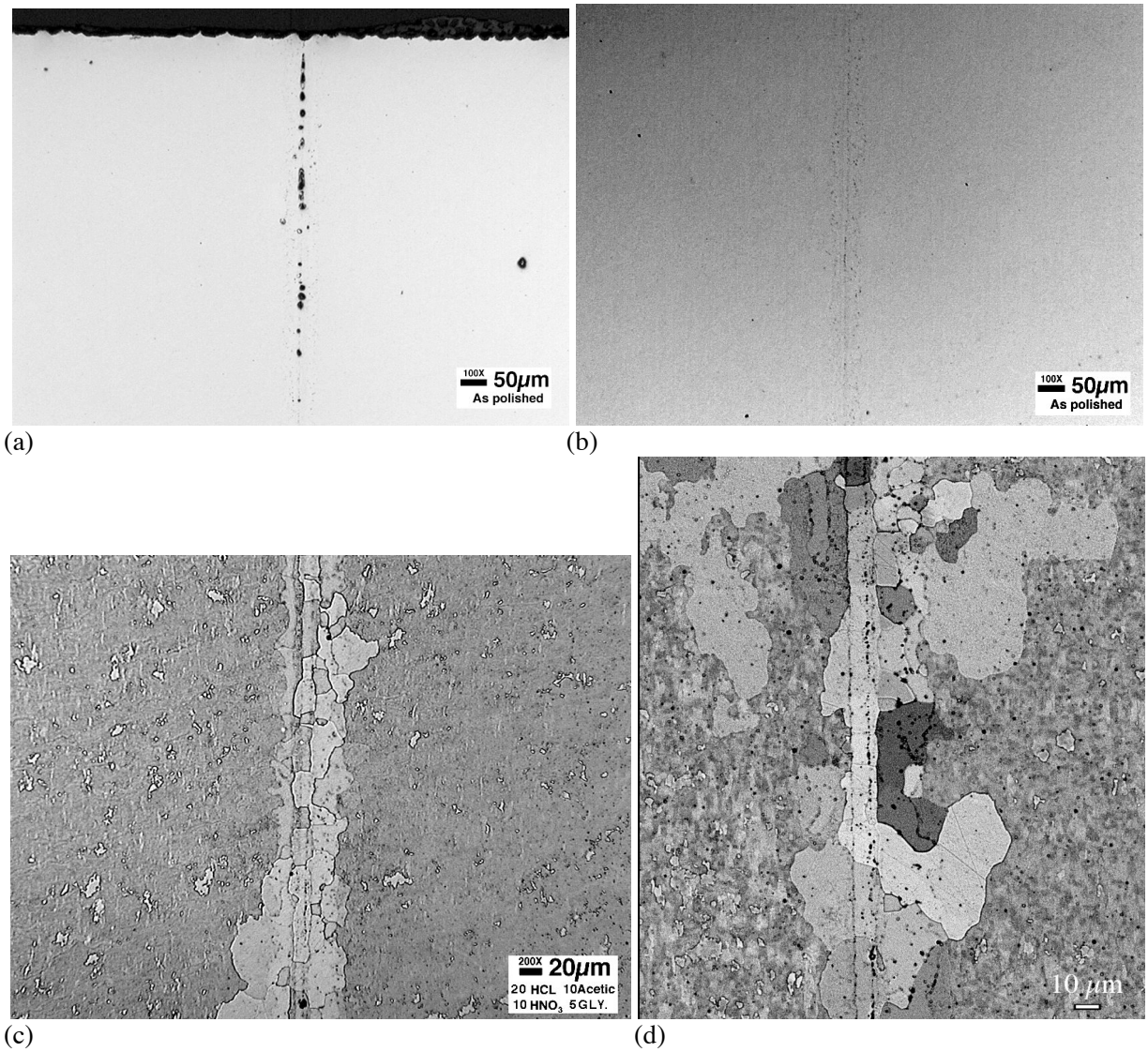


(a) (b)

(c) (d)

Figure 1. Joint made in unrecrystallized alloy PM2000 using the original TLP foil, after a recrystallization anneal for 1 h at 1380°C a), (b), optical images of unetched cross sections; (c) optical image of an etched cross section; (d) SEM BSE image of a cross section.

associated with yttrium-aluminum garnet (YAG) particles, reported earlier after joining and after annealing for 4h at 1000°C [17], were absent, indicating that their presence was an artifact of the point in the processing at which the joints had been examined.

Figure 2 illustrates concentration profiles [made using an electron probe microanalyzer (EPMA)] from the bond line into the alloy for the major elements of interest. Note that, until intellectual property issues concerning the composition of the TLP phase are resolved, its key elements will be denoted 'X' and 'Z.' Two such line scans were made, and both showed a uniform reduction in concentration of elements X and Z over 450 and 650 $\mu$m, respectively, confirming increased diffusion away from the bond (these data are summarized in Table I). The distances over which diffusion occurred were much greater than the depth to which recrystallization was observed near the joint; in both line scans, changes were apparent over a distance of approximately 100 $\mu$m either side of the bond line. The alloy Al concentration adjacent to the bond decreased by a maximum of approximately 1 at% (Fig. 2a), and there was a corresponding increase in Fe concentration (not shown), but such variations were within the range of variations observed periodically throughout the bulk of the alloy, and so are probably not meaningful. Overall, the observed

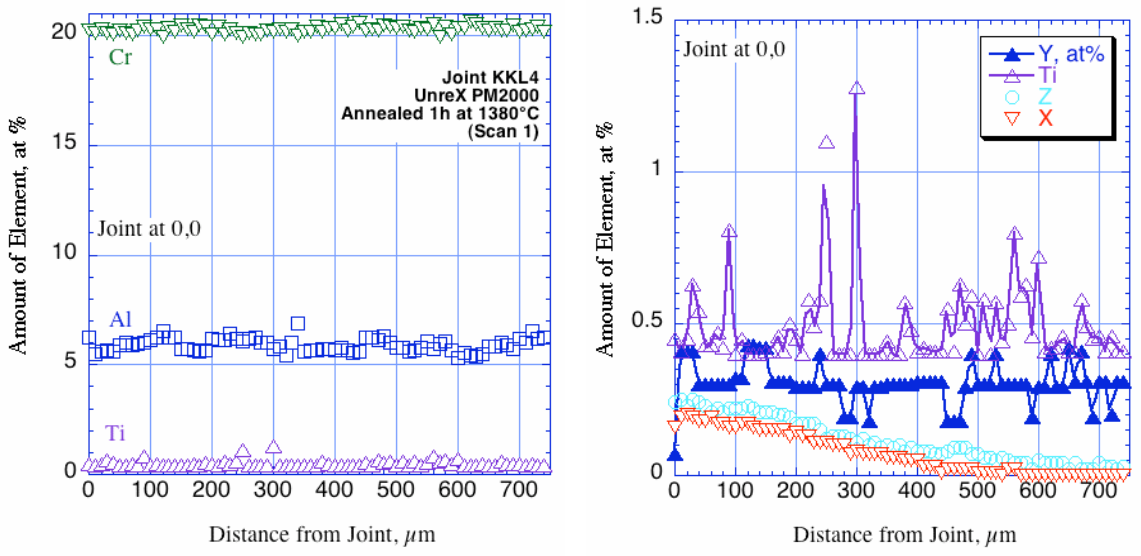


(a) (b)

Figure 2. EPMA concentration profiles through TLP joint made in unrecrystallized alloy PM2000 using the original TLP foil, after a recrystallization anneal for 1 h at 1380°C (a), (b) major and minor elements, Scan 1.

Table I. Depth of Diffusion of TLP Elements

| Condition | Conc. At Joint, at% | | Diffusion Depth, μm | |
|---|---|---|---|---|
| | X | Z | X | Z |
| *PM2000, KKL4, Original TLP Foil* | | | | |
| As Joined | 0.3 (2.0)* | 2.5 | 170 | 80 |
| 4h at 1000°C | ≈1.0 (5.2)* | 1.2 | 270 | 150 |
| 1h at 1380°C | 0.15 | 0.24 | 450 | 650 |
| *PM2000, KKL6, Original TLP Foil* | | | | |
| As Joined | 0.4 (71)* | 2.1 | 90 | 50 |
| 4h at 1000°C | 1.1 (1.25)* | 0.8 | 150 | 150 |
| 1h at 1380°C | — | — | — | — |
| *PM2000, KKL4, Sputter-Deposited TLP* | | | | |
| As Joined+2h at 1000°C | 0.23 | 0 | >30 | -0- |
| +1h at 1380°C | 0.18 | 0.01 | 530 | -0- |

*X-rich precipitates

recrystallization behavior suggests simply that the heat treatment associated with the original TLP bonding (1h at 800°C, followed by 1h at 1000°C) was sufficient to allow recovery of the alloy to occur, leaving insufficient strain in the alloy to drive recrystallization

The cross sections shown in Fig. 3 are from a bond (butt weld) made using 14 mm diam. rods of unrecrystallized alloy PM2000 (condition KKL4), in which the TLP phase was applied by sputtering from the TLP foil used in the earlier bonding. This route was used as a means of introducing less TLP phase into the alloy surface, and facilitating post-bonding homogenization. The alloy is shown after experiencing heat treatments of 1h at 900°C followed by 2h at 1100°C in Ar-4vol%$H_2$, all under compressive loading, followed by furnace cooling. Unetched, the bond line exhibited what appeared to be a string of small pores (Fig. 3a); SEM images suggested that these features may have been metallographic artifacts (Figs. 3c,d). The overall grain size of the nominally unrecrystallized alloy appeared to be larger

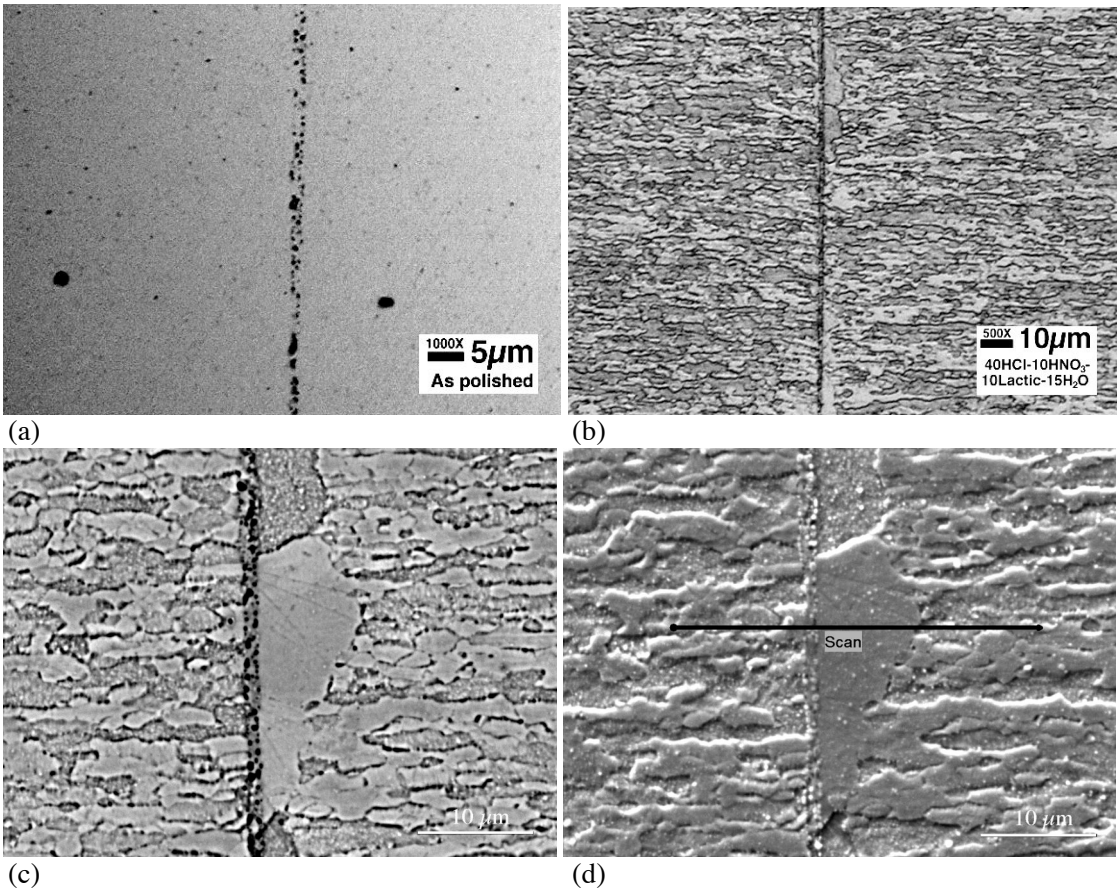


Figure 3. Cross sections of PM2000 (KKL4) after joining and interdiffusion (1h at 900°C plus 2h at 1100°C in Ar-4$H_2$, furnace cool); optical micrographs of unetched (a) and etched (b) cross sections; (c) SEM BSE image; (d) SEM SE image showing location of line scan.

than expected (though full secondary recrystallization had not occurred) and, in a few areas, there were some larger grains associated with the bond line (Figs. 3b-d), similar in appearance to (but smaller than) those seen earlier (Fig. 1c,d). The concentration profiles shown in Fig. 4 are typical of three such profiles that were measured. Surprisingly, the concentration profile for TLP element X was flat; the measured

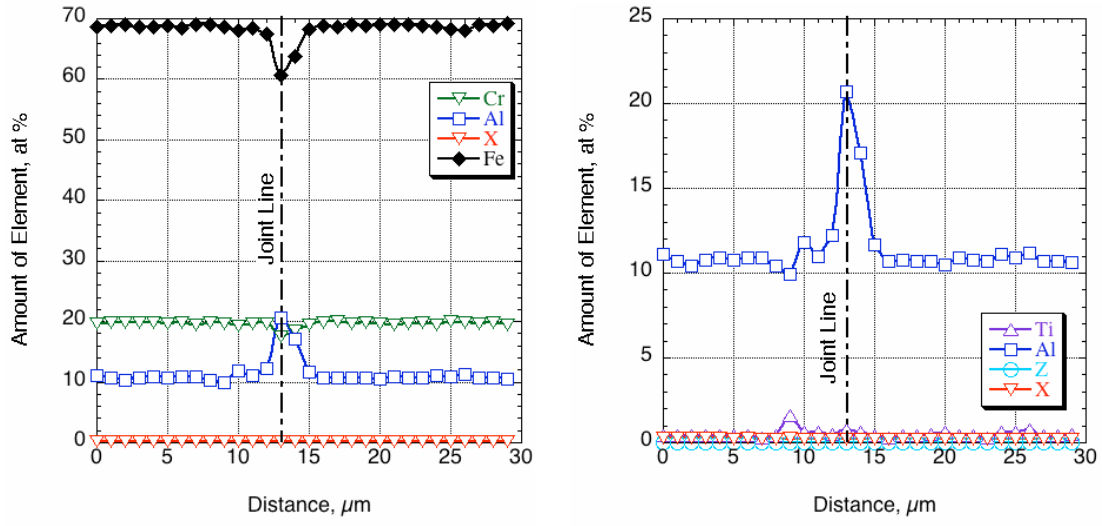


Figure 4. Concentration profiles for (a) major elements; and (b) minor elements along Scan 1.

level was 0.23-0.28 at%, which is directly comparable to those measured for bonds made using the TLP foil, but there were no areas of excess element X in the form of large precipitates. The measured level of TLP element Z was essentially zero, suggesting that the composition of the TLP alloy had been changed as a result of the sputtering process. The other notable feature of these concentration profiles was the presence of an Al peak along the bond line, reaching 21 at%, in places (Fig. 4b). On average, the measured composition of the bond line was: 63.0Fe-18.0Cr-18.0Al-0.67Ti-0.23X, while the bulk alloy was: 68.8Fe-19.8Cr-10.7Al-0.37Ti-0.28X (in at%), indicating an enrichment in Al and Ti, and a decrease in Fe and Cr at the bond line. Previously, precipitates consisting of mixtures of $Al_2O_3$ and TiC have been found along bond lines in this alloy (by transmission electron microscopy [18]), presumably formed by reactions during bonding; no TEM nor analyses for O or C were made on this specimen. These concentration profiles did not extend sufficient distance to determine the depth to which element X had penetrated into the alloy.

Figure 5 shows micrographs of an additional specimen of this bond that was subjected to the standard recrystallization anneal for alloy PM2000 (1h at 1380°C). Unetched, the bond line appeared to contain fewer voids or second phase particles than that shown in Fig. 3a. The etched cross section in Fig. 5c indicates a string of small, recrystallized grains extending up to 30 $\mu$m either side of the bond line, similar to those shown in Fig. 1, while the structure of the bulk of the alloy could not be determined using current

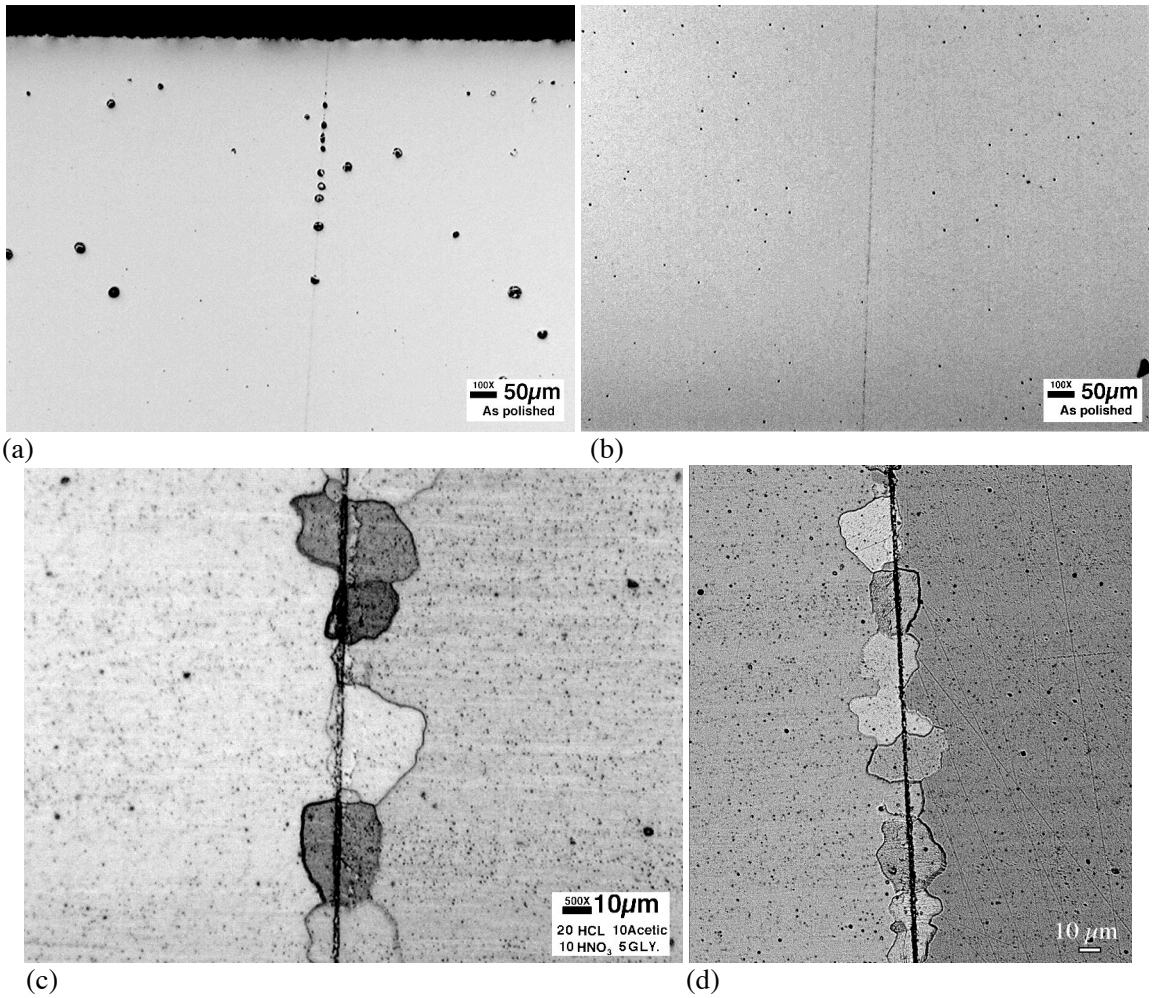


Figure 5. Cross section of TLP joint after joining + interdiffusion + recrystallization anneal (1h at 900°C/2h at 1100°C plus 1h at 1380°C in Ar-4$H_2$, furnace cool). (a),(b) optical micrographs of unetched joint; (c) optical micrographs of etched joint; (d) SEM SE image of cross section.

etching techniques; no grain boundaries were revealed, but it was considered unlikely that the alloy had fully recrystallized. There appeared to be separate large grains either side of the bond line. The EPMA concentration profiles through the joint, shown in Fig. 6, indicate that the concentration of element X decreases from 0.18 at% at the bond line to 0.01at% over 530 $\mu$m, which is very similar to the profile measured on the specimen bonded using the TLP foil, as summarized in Table I. Figure 6b also indicates the continuing presence of Al and Ti enrichments at the bond line, with significant depletions of Al in a zone up to 10 $\mu$m either side of the bond line. Those depletions coincided with enrichments in Ti, Cr, or Fe, but there was no consistent pattern. While this bond appears to be metallurgically sound, the disruption in grain structure across the bond would be expected to degrade its creep strength. One possible route for promoting secondary recrystallization though the bond may be to introduce some level of cold work into the alloy by rolling, immediately after bonding.

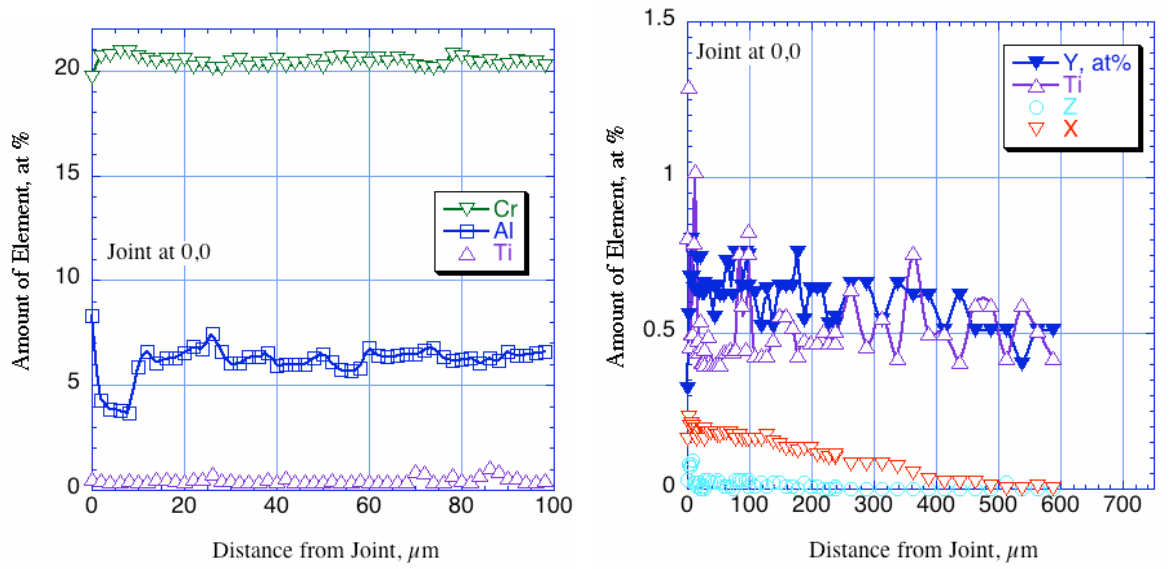


(a) (b)

Figure 6. EPMA concentration profiles on one side of a TLP joint (a) major elements, Scan 1; (b) minor elements, Scan 2.

Since application to the surfaces to be bonded by sputtering resulted in the apparent loss of one of the constituents of the TLP, it was anticipated that the melting temperature of the TLP would be higher than desired. In a further attempt to provide the desired TLP composition in a form of a foil, a new batch of TLP has been processed, using revised procedures to eliminate the use of lubricants that may leave a residue in the foil. In addition, a new compression platform has been built for use on an Instron machine to provide better control of specimen assembly and testing. This platform is shown schematically in Fig. 7. Compromises inherent in using this approach (instead of the controlled atmosphere, hot-pressing equipment used earlier) is that the joining occurs in air, with the attendant issues of oxide filming of the surfaces to be joined, and temperature limitations that (at present) preclude joining and secondary recrystallization in one step.

Pulsed Plasma-Assisted Diffusion Bonding

The compression rig used for PPAD bonding by MER Corp. [19] is shown schematically in Fig. 8. The conditions used for bonding were 9V, 1200A, 62Hz, 70% duty cycle at a constant temperature. Joining was carried out in an Ar atmosphere. The temperature range used in the experiments was from 1170-1380°C, the latter conditions intended to promote secondary recrystallization following bonding. The bond and associated alloy microstructure were examined by metallography and, where secondary recrystallization had not been accomplished during bonding, specimens were given a further heat treatment (1h at 1380°C in air), but no further strain was applied to the specimens. The joining process

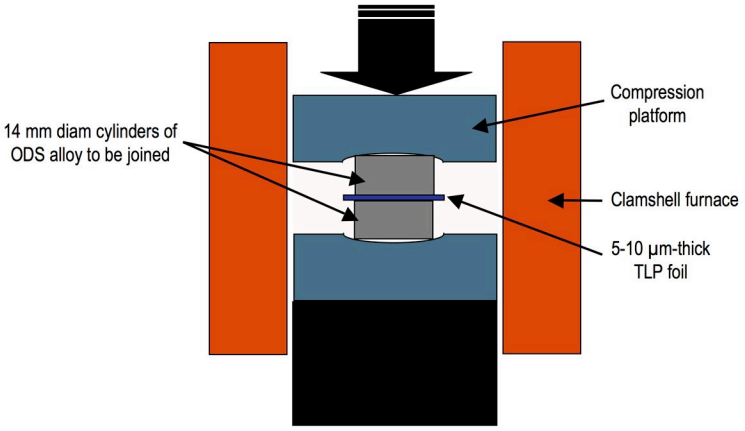


Figure 7. Revised compression platform for TLP bonding

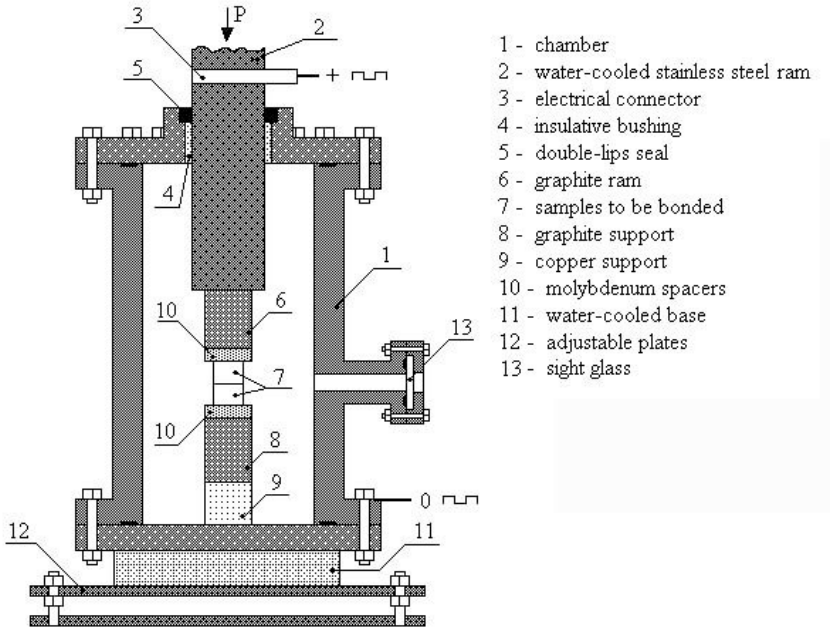


Figure 8. Schematic diagram of rig used for pulsed plasma assisted diffusion bonding of unsupported work pieces.

cycle involved the application of a compressive force of 5 to 12.5MPa perpendicular to the joint while the samples were heated. Micro-plasma discharges between the two halves of the joint resulted in local redistribution of material in the vicinity of the interface, and disruption of any surface oxide layer present on the faces being joined.

The specimens used for making butt joints by PPAD bonding were 19 mm diameter rods of as-extruded PM2000, which was used in the fine-grained condition (Plansee specification KKL4), with no secondary recrystallization. The mating faces were ground to a 1200 grit (U.S.) finish, and ultrasonically cleaned sequentially in acetone and ethanol before joining. Optical micrographs of cross-sections across various joints are shown in Fig. 9. During secondary recrystallization, grain growth occurred through the original interface, which was still delineated as a fine line, as shown in the micrographs, and in more detail in Fig. 10a. These bonds were further examined by transmission electron microscopy (TEM)[20]. Figure 10b is a bright-field TEM micrograph of a sample cut across the bonded interface, which runs down the center of

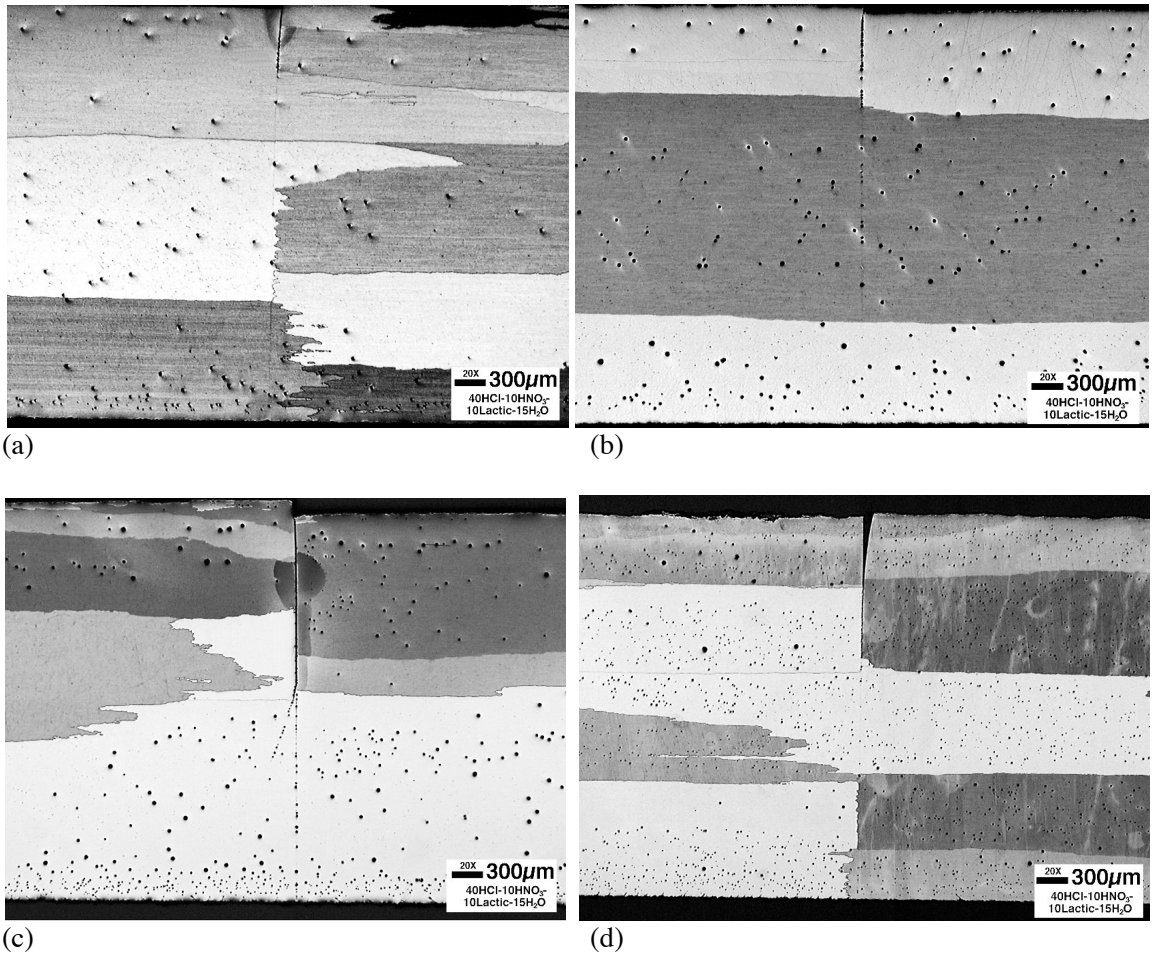


Figure 9. Optical micrographs of etched cross-sections through PPAD-bonded joints. The load to cause failure in the creep test was (a) 77.3 MPa; (b) 76 MPa; (c) 46.7 MPa; and (d) 36.1 MPa.

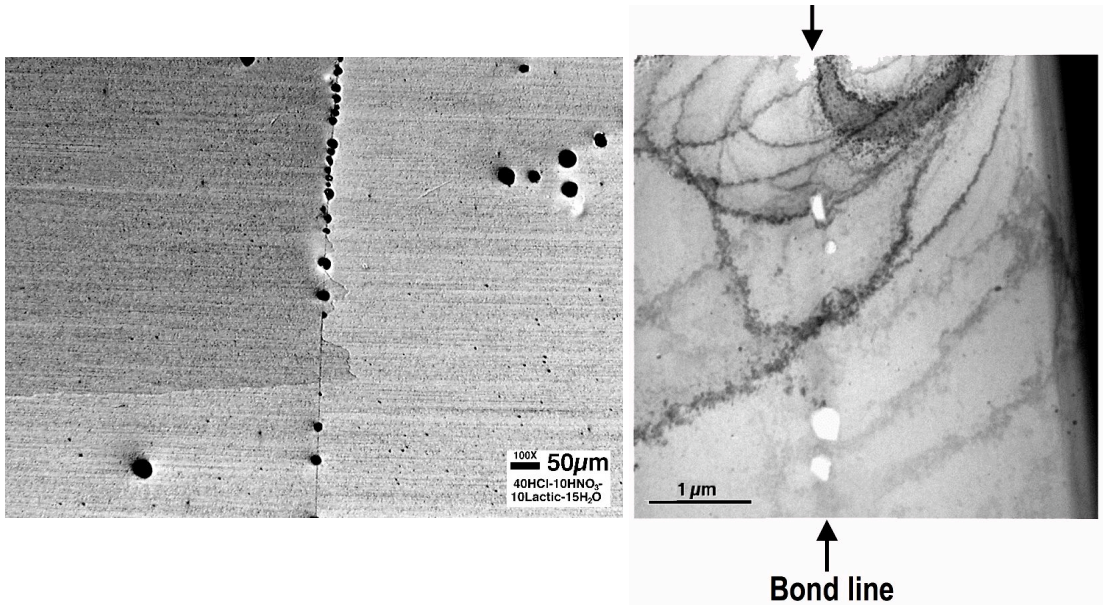


Figure 10. (a) Optical micrograph, and (b) corresponding bright field TEM image of the original bond line, showing that the line of apparent porosity is actually a line of bright alumina particles.

the micrograph. The original interface is marked by a string of white-appearing particles, which would explain the contrast seen in the optical images. The dark bands crossing the micrograph (Fig. 10b) are artifacts (bend contours) caused by changes in the electron diffraction conditions that occur as the TEM sample distorts under its own weight. However, the continuity of these contours across the interface indicates that the alloy grain spanning the interface is a single crystal. The slight darkening along the line of the interface was due to thickness variations across the sample: the sample was slightly thicker at the interface than in the surrounding area, since the hard oxide particles at the interface thinned more slowly than the matrix, but also shielded the adjacent region from the ion beam. The particles along the interface had a separation of between 0.5 and 2 $\mu$m and a typical size of about 0.2 $\mu$m. The variation in spacing of the particles may influence the ease with which the grain boundaries move through the interface during recrystallization, hence explaining some of the serrations along the boundaries seen in Figs. 9 and 10.

The particles found along the interface were examined by energy-dispersive X-ray analysis, and all gave similar spectra that corresponded to almost pure aluminum oxide. In some cases a small Y signal was observed, most likely due to the presence of small Y-rich particles in the vicinity of the alumina. The fine dispersion of Y or yttrium-aluminum oxide particles found throughout the sample were in the size range of 20-30nm, and larger alumina or carbide particles occasionally were present. Since the distribution of the non-interfacial particles in the alloy was similar in both the region near the interface and well away from it, their distribution did not appear to have been affected by the bonding process. Overall, the microstructure shown in Fig. 10 clearly demonstrates that PPAD bonding has produced a sound joint in alloy PM2000.

The strength of the joints so produced was measured in an incrementally-loaded creep test at 1000°C in air. Miniature shoulder-loaded, dog bone-shaped creep specimens were cut from the butt-joined cylinders by electro-discharge machining; Fig. 11 indicates how the specimens were oriented and their dimensions.

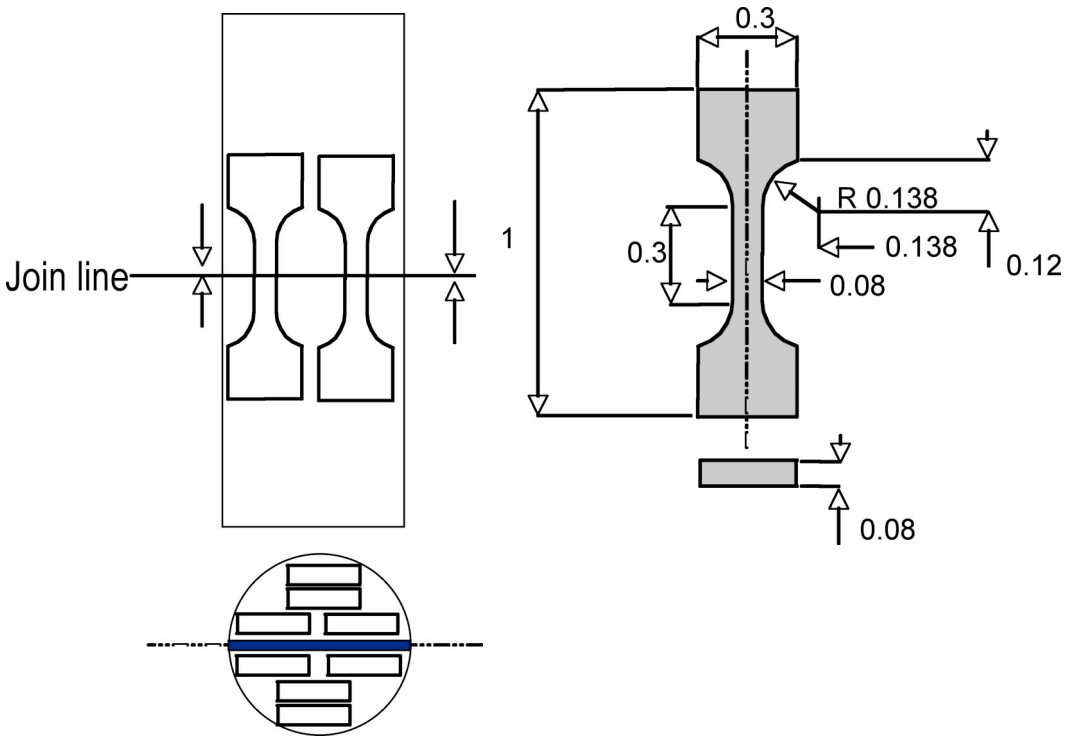


Figure 11. Miniature creep specimens used in the incrementally-loaded creep test, showing (a) orientation of specimens cut from butt-joined cylinders; and (b) specimen dimensions (in inches).

The creep tests used dead weight loading, which was increased in increments of 5 MPa, typically once per day, until obvious creep was observed, or failure occurred. Figure 12a summarizes the loads at failure as a function of PPAD processing temperature, and Fig. 12b compares the loads at failure with those for recrystallized monolithic specimens made from the same bar stock. The best joints exhibited joint strength factors (JSFs) of 82%. For high creep-strength ferritic steels joined by conventional welding methods, typical JSF values are 50-80%, and for weldable high-temperature Ni-base alloys, values of approximately 80% are considered acceptable [21,22].

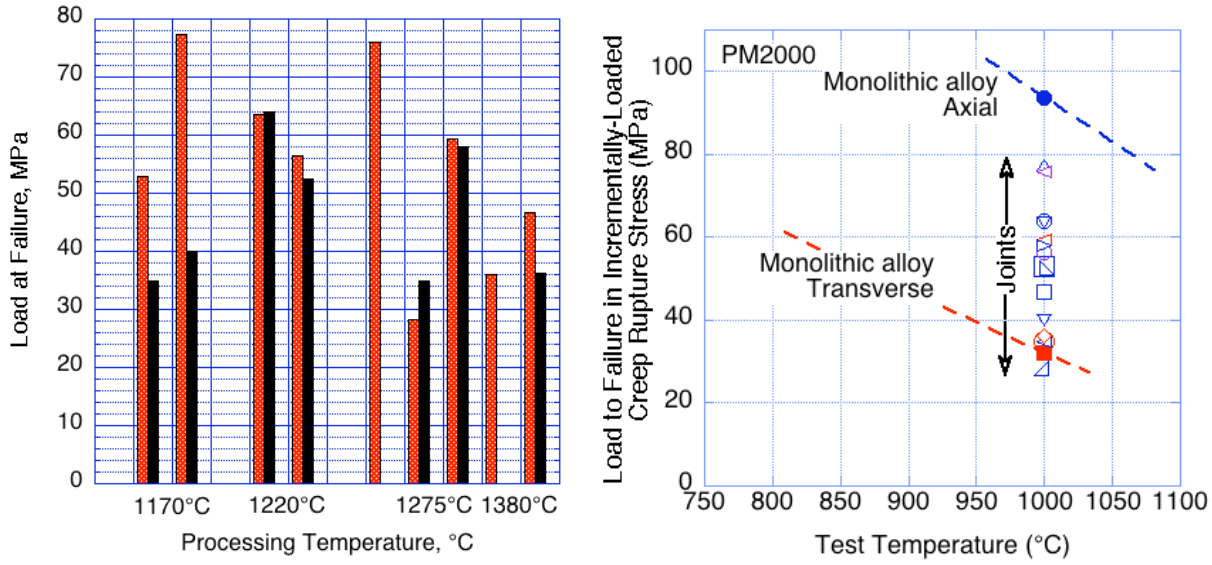


(a) (b)

Figure 12. Summary of the creep strengths of butt joints in PM2000 made by PPAD bonding (a) bar chart showing results for duplicate specimens as a function of processing temperature; (b) comparison with the axial and transverse creep strengths for monolithic specimens from the same starting material.

The failures in these joints apparently did not initiate along the bond line, but often in the vicinity of a grain boundary, as shown in Fig. 13. The observed mode of failure was by crack-initiated transgranular brittle fracture, followed by ductile overload failure, which is typical for this alloy [23,24]. Because of the large grain size in these miniature specimens, the gauge of the specimen shown was essentially two grains wide. Typically, cracking initiated in one grain, causing the other to fail by overloading. There was a limited amount of porosity present in the samples, and this did not increase noticeably during the testing.

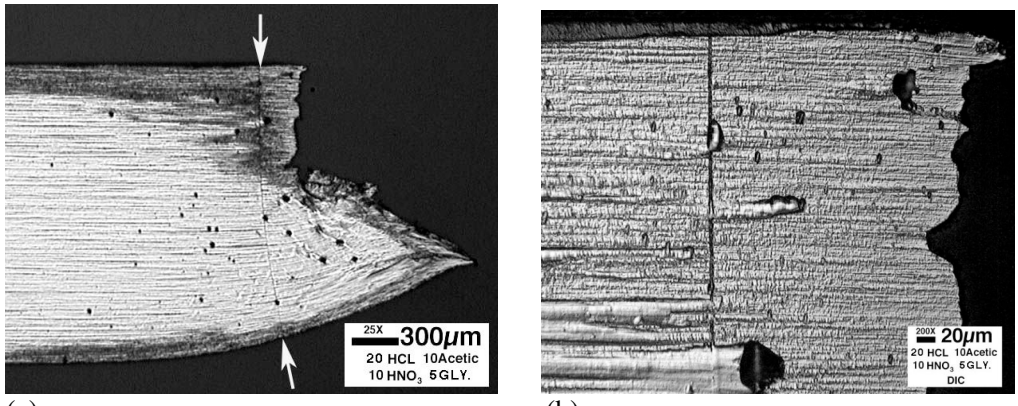


(a) (b)

Figure 13. Heavily-etched cross sections of failed butt joints, illustrating that failure did not occur in the bond line (a) classic brittle/ductile failure, with the bond line shown by arrows; and (b) enlarged view of the top part of the fracture surface shown in (a).

## OXIDATION-LIMITED SERVICE LIFETIME

Key parameters needed for analytical modeling to predict the oxidation-limited service lifetime of ODS-FeCrAl alloys are accurate values for the oxidation rate (as a function of temperature and environment), the initial Al reservoir of the alloy [Al content ($C_B$) and volume of the part subject to oxidation ($\underline{V}$)], and the minimum residual Al content at which protective scale formation is no longer supported ($C_{B^*}$).

Oxidation-limited lifetime data have been generated for relevant ODS alloys, as well as other FeCrAlY-type compositions made by conventional processing; the alloys tested are listed in Table II. Specimens of each alloy with different thicknesses (and shapes) were exposed to provide a range of initial Al reservoir, and run in laboratory air at temperatures from 1000 to 1300°C until failure occurred. Examples of the lifetimes observed for alloys Inconel MA956 and 956HT are shown in Fig. 14 (each data point represents a specimen run to failure), plotted against the parameter component volume/surface area ($V/A$). Note that, at 1100°C, lives up to 23kh were observed, and that exposures at 1000°C have not yet reached times to

Table II. Nominal Compositions of Ferritic ODS Alloys of Interest (atomic percent).

| Alloy | Fe | Cr | Al | Mo | W | Ti | Si | Y | Zr | O | C | S* | N* |
|---|---|---|---|---|---|---|---|---|---|---|---|---|---|
| INCO MA 956 | Bal | 20.05 | 8.77 | 0 | 0.01 | 0.40 | 0.13 | 0.24 | 0 | 0.65 | 0.06 | 41 | 608 |
| | Bal | 19.39 | 8.40 | 0 | 0 | 0.39 | — | 0.30 | — | 0.66 | 0.04 | 180 | — |
| INCO MA956HT | Bal | 21.45 | 11.01 | 0.01 | — | 0.43 | 0.09 | 0.22 | 0 | 0.69 | 0.13 | 80 | 1059 |
| | Bal | 21.72 | 10.66 | 0.01 | 0 | 0.43 | 0.11 | 0.23 | 0 | 0.68 | 0.17 | 71 | 1064 |
| PM2000 | Bal | 18.91 | 9.82 | 0.01 | 0.01 | 0.49 | 0.07 | 0.22 | 0 | 0.81 | 0.04 | 34 | 104 |
| | Bal | 20.02 | 10.62 | 0 | 0 | 0.44 | 0.04 | 0.23 | 0 | 0.74 | 0.03 | 50 | 211 |
| Dour Alloy ODM 751 | Bal | 16.13 | 9.62 | 0.82 | 0 | 0.61 | 0.07 | 0.24 | 0 | 1.58 | 0.03 | 93 | 893 |
| | Bal | 16.36 | 7.57 | 0.85 | 0 | 0.65 | 0.11 | 0.24 | 0 | 1.62 | 0.03 | 82 | 918 |
| ODS-$Fe_3Al$ (PMWY1) | Bal | 2.39 | 25.93 | — | — | 0.01 | 0.07 | 0.20 | 0 | 0.96 | 0.24 | 33 | 3300 |
| ODS-$Fe_3Al$ (PMWY2) | Bal | 2.13 | 27.07 | — | — | 0 | 0.05 | 0.21 | 0 | 0.62 | 0.16 | 30 | 3480 |
| ODS-$Fe_3Al$ (PMWY3) | Bal | 2.14 | 27.29 | — | — | 0 | 0.07 | 0.22 | 0 | 0.43 | 0.12 | 24 | 150 |
| Kanthal APM | Bal | 20.37 | 10.65 | — | — | 0.03 | 0.43 | 0 | 0.06 | 0.17 | 0.13 | 16 | — |
| Kanthal APMT** | Bal | 21.33 | 9.74 | 1.55 | 0 | 0.02 | 1.11 | 0.15 | 0.06 | 0.17 | 0.13 | 0 | 1512 |
| | Bal | 21.43 | 9.3 | 1.51 | 0 | 0.02 | 0.88 | 0.13 | 0.06 | 0.17 | 0.16 | 0 | 1979 |

*ppma
**+0.07Hf

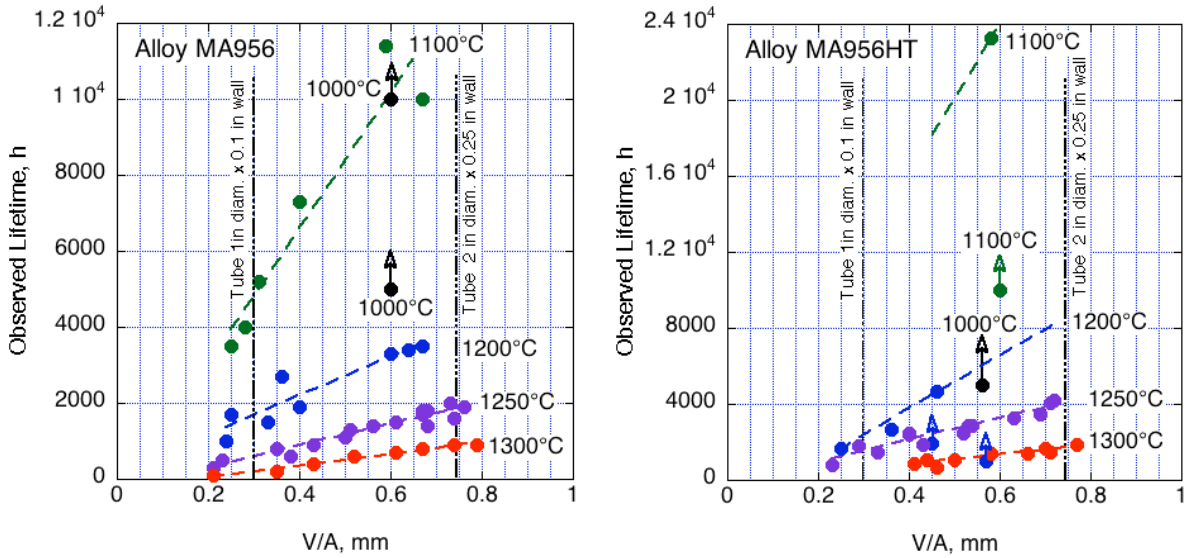


(a) (b)

Figure 14. Summary of cyclic oxidation exposures in air, run to failure at each of four temperatures, for (a) alloy MA956; and (b) alloy MA956HT.

produce failures. The value of *V/A* for a tube of 1 in diam. and 0.1 in wall thickness is 0.3, and 0.75 for a tube of 2 in diam. and 0.25 in wall thickness. The oxidation lifetime for MA956HT was found to be significantly longer than for MA956. While the major nominal difference is the increased Al level ($C_B$) in MA956HT, the measured oxidation kinetics for MA956HT were, in fact, slower than for MA956, while the extent of scale spallation was similar. Thus, the longer lifetime was not only the result of a larger reservoir of Al, but also because of a lower rate of Al consumption.

For a given value of *V/A*, algorithms for lifetime as a function of temperature can be obtained from plots such as that shown in Fig. 15. However, this approach does not provide flexibility for including effects of changes in *V/A*, oxidation rate, and variations in $C_{B^*}$, for which new data are needed for each new condition considered. Instead, a simple model [25] based on earlier work [15,16] was used to relate service life (time to breakaway, $t_b$) to the quantity (Al available for oxidation) / (oxidation rate). The input parameters needed are those that describe the oxidation kinetics of each alloy (Arrhenius data for calculating the temperature-dependence of the oxidation rate); and Al reservoir data (initial mass fraction of Al in the alloy, $C_{Bo}$; mass fraction of Al in the alloy at which a protective $Al_2O_3$ can no longer form, $C_{B^*}$; and the densities of the alloy and alumina). Using this approach, calculation of the oxidation-limited lifetime requires simply input of alloy temperature, and the area and volume of alloy exposed.

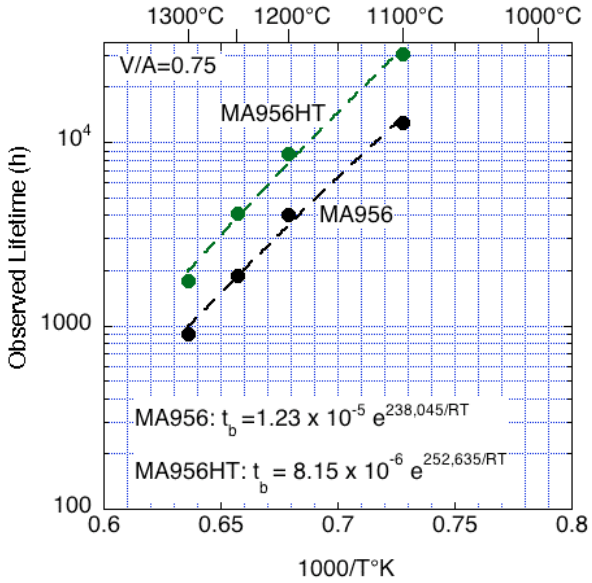


Figure 15. Temperature-dependence of oxidation-limited lifetimes for alloys MA956 and MA956HT (in the algorithms shown, $t_b$ is in hours; T is in °K, and R = 8.314 $Jmole^{-1}K^{-1}$).

Efforts have continued to measure values of oxidation kinetics and $C_{B^*}$ by means of specimens exposed until oxidation failure occurred. During the course of these measurements, it became clear that the basic assumption made in the model—that the Al concentration gradient through the specimen remains flat—is not always valid, and that local scale spallation can result in Al concentration gradients, and an increased rate of consumption of Al [26]. Geometrical/shape factors appear to be important, with the shape most subject to scale spallation being the parallelepiped used for standard oxidation specimens. As a result, data were collected from concentration profiles measured at the center of standard specimens (which typically did not fail first), and at the ends (which were most susceptible to spallation). Data from such measurements are summarized for alloys Inconel MA956 and 956HT in Figs. 16 and 17; the data for both alloys were essentially indistinguishable, so that the overall trends deduced reflect all of the data.

From these plots, the point at which the alumina scale was no longer protective was taken to be that at which Cr started to be oxidized, that is, the Al concentration corresponding to the point where the Cr concentration profile started to decrease. The overall result was that the deduced value of $C_{B^*}$ ranged from ≈ 0.2 at% at the specimen centers (no spallation), to 0.5at% at the specimen ends for the standard

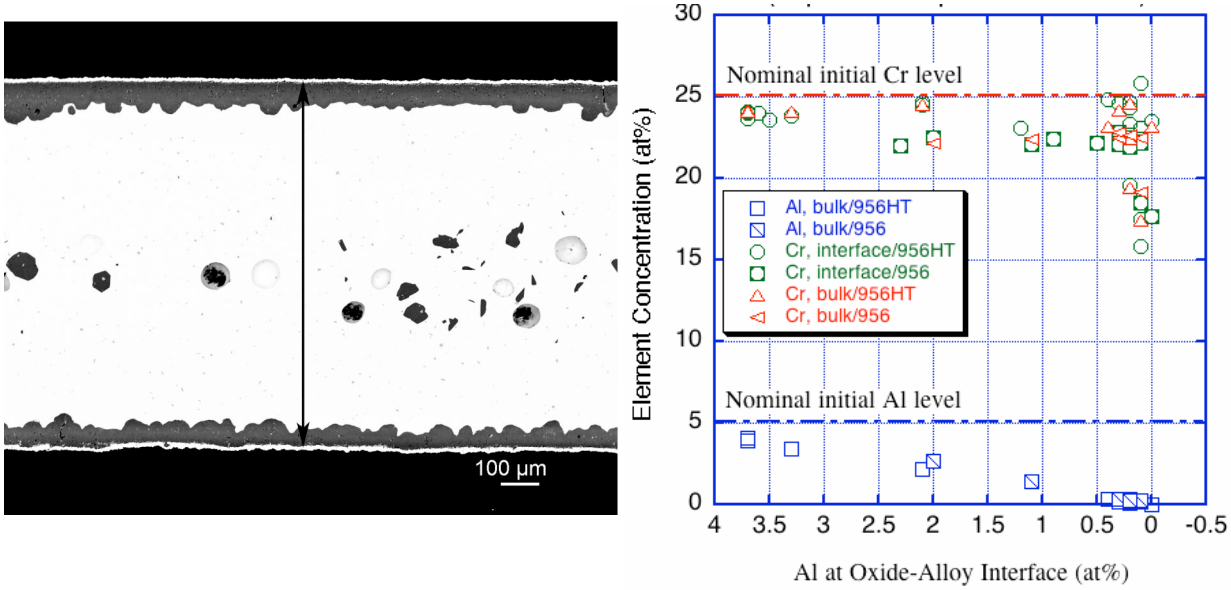


(a) (b)

Figure 16. Measurement of minimum Al for protective behavior ($C_{B^*}$) for MA956 and MA956HT (a) cross section of the center of a specimen of MA956 oxidized to failure at 1200°C; and (b) plot of corresponding Al and Cr concentrations measured at the metal-oxide interface in the central region of multiple specimens oxidized to failure at 1200°C.

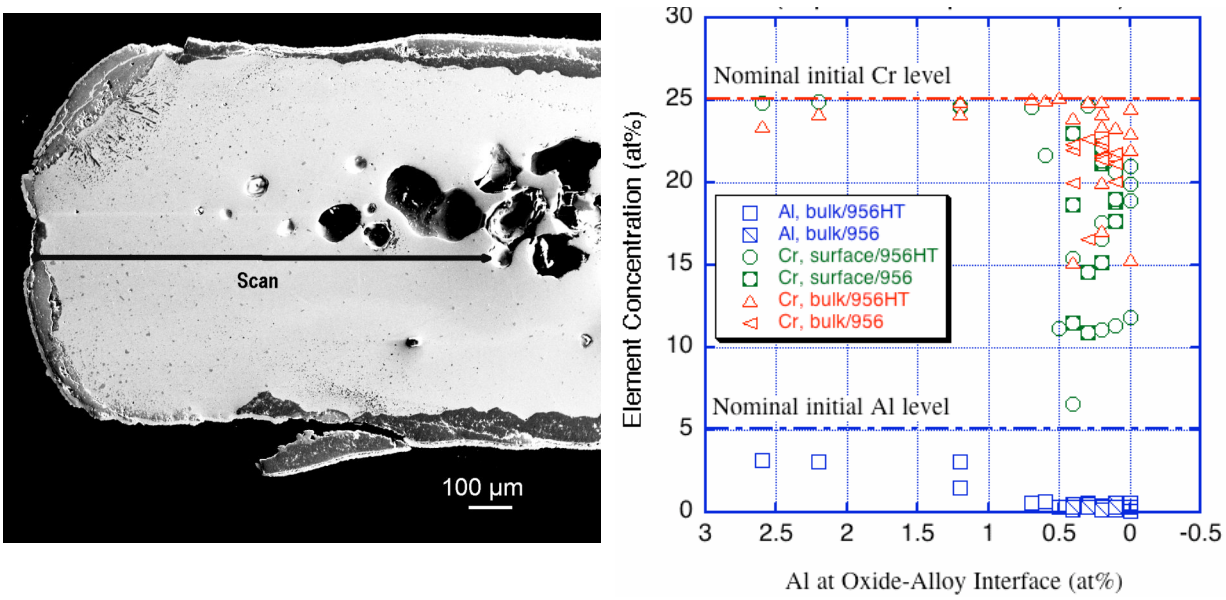


(a) (b)

Figure 17. Measurement of minimum Al for protective behavior ($C_{B^*}$) for MA956 (a) cross section of the end of a specimen of MA956 and MA956HT oxidized to failure at 1200°C; and (b) plot of corresponding Al and Cr concentrations measured at the metal-oxide interface at the ends of multiple specimens oxidized to failure at 1200°C.

parallelepiped oxidation specimen. When used in the simple two-stage model for MA956 [26], the value of 0.5at% gave an excellent fit to the observed lifetimes shown in Fig. 14a (which were generated using standard specimens). However, the same value of $C_{B^*}$ underestimated the observed lifetimes for MA956HT (Fig. 14b) which were generated using disc-shaped specimens, whereas a value of 0.2 at% provided a closer fit, suggesting that there was some contribution to Al loss by scale spallation from the disc specimens, but not as much as from the parallelepipeds.

## SUMMARY

Two techniques for joining ODS alloys have shown good promise. Transient liquid-phase diffusion bonding, using a thin foil of low-melting TLP alloy, produces what appear to be clean joints. The initial, unexpected, microstructural features can be explained by considerations of the local concentration and transport of the TLP phases away from the joint with time and temperature. Heat treatments have resulted in acceptable dispersion of the TLP constituents after joining. A continuing issue is that it appears that the thermal histories associated with the TLP processing routes used so far have diminished the driving force for post-joining, secondary recrystallization of the alloy to form the desired large aspect-ratio grain structure. Re-evaluation of the processing steps in the TLP joining process for compatibility with a secondary recrystallization step is the next goal.

Interaction with MER Corporation has determined the appropriate processing parameters to produce very promising butt joints by pulsed plasma-assisted diffusion bonding. When secondary recrystallization after bonding resulted in grain growth through the bond line, joint strengths up to 82% of the bulk parent alloy were measured in creep tests in air at 1000°C. This technique is ready for demonstration on appropriate components (tubes), and the next step should be to measure standard creep data using exemplar joints in specimens taken from bonded tubes.

The completion of some of the long-term oxidation lifetime tests of ODS-FeCrAl alloys has produced not only data against which the predictions of the analytical model can be compared, but also values of a key parameter needed by the oxidation lifetime model. As the exposures of full sets of specimens of a given alloy complete testing, it will be possible to reevaluate the overall oxidation kinetics for use with the new parameter values in a refined version of the model. While it is considered that the assumptions embodied in the model are satisfactory for application to oxides grown on tubes, edge/end effects and specimen shape (which are more important for components made from plate or sheet) have been noted to give rise to Al concentration gradients that can significantly reduce oxidation lifetime. The effects of environments other than air on oxidation lifetime also need to be considered, since constituents such as water vapor or $CO_2$ in the environment could modify the mode and/or rate of oxide growth.

## ACKNOWLEDGMENTS

This research was sponsored by the Fossil Energy Advanced Research Materials (ARM) Program, U.S. Department of Energy, under contract DE-AC05-96OR22464 with UT-Battelle LLC. The authors thank the director of the ARM program, Robert Romanosky, of the National Energy Technology Laboratory, and Roddie Judkins, Director of the Fossil Energy program at ORNL, for their continued enthusiasm and support. We also thank Hu Longmire for developing metallographic preparation skills for ODS-FeCrAl alloys; Larry Walker for electron microprobe analysis expertise; Dorothy Coffey for her skill with focused ion-beam milling to produce the TEM samples; John Shingledecker and Ralph Martin for advice and assistance with creep testing; and Jim Keiser for reviewing the manuscript.

## REFERENCES

1. See, for instance, I.G. Wright, B.A. Pint, and Z.P. Lu, "Overview of ODS alloy development," Proc. 19th Annual Conference on Fossil Energy Materials, Knoxville, Tennessee, 9th-11th May 2005.
2. J.P. Hurley, "Applications for Dispersion-Strengthened Alloys in Thermal Power Systems," Proc. 21st Annual Conference on Fossil Energy Materials, Knoxville, Tennessee, 30th April–2nd May 2007.
3. Private communication, D. Arrell (Siemens Power Generation, Inc.) to I.G. Wright (ORNL), May 2007.
4. See, for instance, "Incoloy® alloy MA956," Special Metals Corporation Technical Bulletin No. SMC-008 (2004).

5. H.D. Hedrich, H.D. Mayer, G. Haufler, M. Kopf, and N. Reheis, "Joining of ODS Superalloys," pp. 789-798 in *Proc. Conf. on Materials for Advanced Power Engineering,* D. Coutsouradis, J.H. Davidson, J. Ewald, P. Greenfield, T. Khan, M. Malik, D.B. Meadowcroft, V. Regis, R.B. Scarlin, F. Schubert, and D.V. Thornton, Eds., Kluwer Academic Publishers, Dordrecht (1994).
6. M.A. Harper, *Development of ODS Heat Exchanger Tubing*, Special Metals Corporation, Huntington, KY, April 2003.
7. M.G. McKimpson and D. O'Donnell, "Joining ODS materials for high-temperature applications," *JOM,* 46, (7), 49-51 (1994).
8. T.I. Kahn and E.R Wallach, "Transient liquid-phase diffusion bonding and associated recrystallization phenomenon when joining ODS ferritic superalloys," *J. Mater, Sci*., 31 (11), 2937-2943 (1996).
9. W.F. Gale and D.A. Butts, "Transient Liquid Phase Bonding," *Sci. and Techn. of Welding and Joining*, 9 (4), 283-300 (2004).
10. V.G. Krishnardula, N.I. Sofrijon, W.F. Gale, and J.W. Fergus, "Transient Liquid-Phase Bonding of Ferritic Oxide Dispersion-Strengthened Alloys," *Met. Mat. Trans. A*, 37, 407-500 (2006).
11. C.Y. Kang, T.H. North, and D.D. Petrovic, "Microstructural features of friction-welded MA 956 superalloy material," *Met. Mat. Trans. A*, 27, 4019-4029 (1996)
12. P.D. Sketchley, P.L. Threadgill, and I.G. Wright, "Rotary friction welding of an $Fe_3Al$-based ODS alloy," *Mat. Sci. & Eng. A-Structural Materials Properties, Microstructures, and Processing*, Special Issue, 329, 756-762 (2002).
13. V.G. Krishnardula, R. Aluru, N.I. Sofyan, J.W. Fergus, W.F. Gale, "Solid-State Diffusion Bonding of MA956 and PM2000," pp. 885-888 in *Trends in Welding Research,* Proc. 7th Intl. Conf., S.A. David, T. DebRoy, J.C. Lippold, H.B. Smartt, and J.M. Vitek, Eds., ASM (2005).
14. K. Nishimoto, K. Saida, and R. Tsuduki, "Effect of pulsed electric-current on densification behavior of bonded interlayer of oxide dispersion-strengthened superalloys," pp. 747-755 in *Joint. J. Japan Institute of Metals*, 65, No. 8 (2001).
15. W. J. Quadakkers and K. Bongartz, "The prediction of breakaway oxidation for alumina-forming ODS alloys using oxidation diagrams," *Werkstoffe und Korrosion*, 45, 232-41 (1994).
16. M. J. Bennett, H. Romary and J. B. Price, "The Oxidation Behavior of Alumina-Forming Oxide Dispersion-Strengthened Ferritic Alloys at 1200-1400°C," pp. 95-103 in *Heat-Resistant Materials*, K. Natesan and D. J. Tillack, eds. (ASM, Materials Park, Ohio, 1991).
17. I.G. Wright, N.S. Bornstein, E.G. Dyadko, and S.N. Dryepondt, "Enabling The Practical Application Of Oxide Dispersion-Strengthened Ferritic Steels," Proc. 20th Annual Conference on Fossil Energy Materials, Knoxville, Tennessee, 24th-26th April 2006.
18. I.G. Wright, B.A. Pint, C.G. McKamey, "ODS alloy development," Proc. 17th Annual Conference on Fossil Energy Materials, Knoxville, Tennessee, 22nd-24th April 2003.
19. E.G. Dyadko, "Novel Joining Technique for Oxide Dispersion-Strengthened Iron Aluminide Alloys," Final Report on Contract No. DE-FG03-00ER83041 December, 23, 2006.
20. G.J. Tatlock, E.G. Dyadko, S.N. Dryepondt, and I.G. Wright, "Pulsed Plasma-Assisted Diffusion Bonding of ODS-FeCrAl Alloys," *Met. Mat. Trans. A*, 38A, 1663-5 (2007).
21. See, for instance, J. Schubert, A. Klenk, and K. Maile, "Determination of weld strength factors for the creep rupture strength of welded joints," pp. 792-805 in *Creep & Fracture in High-Temperature Components-Design & Life Assessment Issues*, I.A. Shibli, S.R. Holdsworth, and G. Merkling, Eds., DES*tech* Publications, Inc. (2005).
22. J. P. Shingledecker and I. G. Wright, "Evaluation of the materials technology required for a 760ºC power steam boiler," pp. 107-119 in *Materials for Advanced Power Engineering 2006*, J. Lecomte-Beckers, M. Carton, F. Schubert, and P. J. Ennis, Eds., Schriften des Forschungszentrums Jülich (2006).
23. W.H. Weigert, R.J. Henricks, "Tensile and creep-rupture behavior of two advanced, oxide dispersion-strengthened sheet alloys," pp. 575-584 in *Superalloys 1980*, J.K. Tien, S.T. Wlodek, H. Morrow, M. Gell, and G. R. Maurier, Eds., ASM (1980).
24. J.D. Whittenberger, "Tensile and creep properties of the experimental oxide dispersion-strengthened iron-base sheet alloy MA956 at 1365K," *Met. Trans. A*, 9A, 101-110 (1978).

25. I.G. Wright, B.A. Pint, L.M. Hall, and P.F. Tortorelli, "Oxidation lifetimes: experimental results and modeling," paper presented at the European Federation of Corrosion Workshop on *Lifetime Modeling of High-Temperature Corrosion Processes*," Frankfurt am Main, Germany, February 2001.
26. I.G. Wright, C.G. McKamey, and B.A. Pint, "ODS alloy development," Proc. 16th Annual Conference on Fossil Energy Materials, Baltimore, Maryland, 22nd-24th April 2002.